ADVANCED MATERIALS
www.advmat.de

Room-Temperature All-Liquid-Metal Batteries Based on Fusible Alloys with Regulated Interfacial Chemistry and Wetting

*Yu Ding, Xuelin Guo, Yumin Qian, Leigang Xue, Andrei Dolocan, and Guihua Yu**

Liquid metal batteries are regarded as potential electrochemical systems for stationary energy storage. Currently, all reported liquid metal batteries need to be operated at temperatures above 240 °C to maintain the metallic electrodes in a molten state. Here, an unprecedented room-temperature liquid metal battery employing a sodium–potassium (Na–K) alloy anode and gallium (Ga)-based alloy cathodes is demonstrated. Compared with lead (Pb)- and mercury (Hg)-based liquid metal electrodes, the nontoxic Ga alloys maintain high environmental benignity. On the basis of improved wetting and stabilized interfacial chemistry, such liquid metal batteries deliver stable cycling performance and negligible self-discharge. Different from the conventional interphase between a typical solid electrode and a liquid electrolyte, the interphase between a liquid metal and a liquid electrolyte is directly visualized via advanced 3D chemical analysis. Insights into this new type of liquid electrode/electrolyte interphase reveal its important role in regulating charge carriers and stabilizing the redox chemistry. With facile cell fabrication, simplified battery structures, high safety, and low maintenance costs, room-temperature liquid metal batteries not only show great prospects for widespread applications, but also offer a pathway toward developing innovative energy-storage devices beyond conventional solid-state batteries or high-temperature batteries.

Since the first electrochemical cell was built by Volta in the 1800s, significant progress has been made toward advanced batteries with various combinations of electrodes and electrolytes.[1,2] Alkali metals with low redox potentials and high capacities are regarded as the most promising electrode alternatives to achieve ultrahigh energy density.[3,4] However, the stripping/deposition of alkali metals is compromised by large volume change, serious dendrite growth, and parasitic electrolyte decomposition.[5,6] Up to now, considerable efforts have been made on the design of nanostructured current collectors, novel electrolytes, and artificial solid electrolyte interphase (SEI) to alleviate those problems.[7–9] Additionally, the adoption of liquid metals provides another promising approach to eliminate the intrinsic issues of alkali metals.[10–12] Liquid metals not only provide a platform to synthesize nanomaterials and control crystallization of dissolved species, but also eliminate the dendrite issue of alkali metals given the self-healing properties.[13,14] The development of liquid metal batteries can be traced back to the 1960s, when thermally regenerative cells were invented by pairing alkali metal negative electrodes with other metallic positive electrodes.[15–17] In contrast to solid-state batteries, the self-segregating structure of the liquid metal negative electrode, positive electrode, and electrolyte gives rise to facile and cost-effective cell fabrication. Despite the attractive performance characteristics already demonstrated, including high power and long cycle life, current cells need to be maintained at elevated temperatures to melt the metallic electrodes. Meanwhile, either molten salts or solid electrolytes were employed in the reported liquid metal batteries. The dissolution of alkali metals in molten salts will lead to self-discharge with low Coulombic efficiency, and the fragility of costly solid electrolytes is a vulnerability in practical applications.[15] Therefore the widespread implementation of conventional high-temperature liquid metal batteries is restricted by sophisticated cell design, rigorous thermal management, as well as issues related to sealing and corrosion. Recently, Cui et al. reported an intermediate temperature liquid metal battery with a garnet-based solid electrolyte sandwiched between a molten lithium (Li) negative electrode and a tin–lead (Sn–Pb) or bismuth–lead (Bi–Pb) alloy positive electrode, and the operating temperature was lowered to 240 °C.[18]

Based on the rational screening of fusible alloys and fundamental study on the wetting behavior and interfacial chemistry, we build the first-of-its-kind room-temperature all-liquid-metal battery with the lowest operating temperature ever reported. The gallium–indium (Ga–In) liquid metal alloy positive electrodes versus the sodium–potassium (Na–K) liquid metal alloy negative electrode delivers a stable cycling performance at room temperature, and the cost can be further reduced by using a Ga–Sn alloy-based positive electrode, which demonstrates

Dr. Y. Ding, X. Guo, Dr. Y. Qian, Dr. L. Xue, Dr. A. Dolocan, Prof. G. Yu
Materials Science and Engineering Program
Texas Materials Institute
The University of Texas at Austin
Austin, TX 78712, USA
E-mail: ghyu@austin.utexas.edu

The ORCID identification number(s) for the author(s) of this article can be found under https://doi.org/10.1002/adma.202002577.

DOI: 10.1002/adma.202002577

 © 2020 WILEY-VCH Verlag GmbH & Co. KGaA, Weinheim

comparable electrochemical performance. Moreover, it is possible to achieve even a lower operating temperature at –13 °C when replacing Ga-based binary alloys with the Ga–In–Sn ternary alloy (Galinstan). The self-healing nature of liquid metals renders them immune to structural degradation faced by conventional solid-state electrodes.[19] Meanwhile, liquid metals inherently possess higher densities than conventional electrode materials, offering potential to achieve high capacities. Without auxiliary heating systems, molten salts, and/or solid electrolytes, such room-temperature liquid metal batteries are promising to realize wider applications beyond stationary energy storage.[20]

Metals in general tend to have high melting points in light of strong bonds between the atoms, thus there are very few elemental metals that are liquid at room temperature. Although Hg is molten above –39 °C, its wide utilization is limited by the high toxicity. Therefore eutectic systems provide more freedom for rational screening and selection of fusible alloys to build liquid metal batteries. Besides Hg-based alloys, the fusible alloy family also includes alkali metal-based alloys, Ga-based alloys, and some more complicated multi-element alloys. Table S1, Supporting Information compares the melting point of typical metals and fusible alloys below 100 °C.[21] Taking into account all factors in terms of melting point, natural abundance, environmental benignity, toxicity, and vapor pressure, herein, Na–K alloy as a negative electrode and Ga-based alloys as positive electrodes were selected to enable room-temperature liquid metal batteries, with melting point all below room temperature (–13, 15, 21, and –19 °C for the Na–K, Ga–In, Ga–Sn, and Ga–In–Sn eutectic alloys, respectively). **Figure 1**a shows the schematic of room-temperature all-liquid-metal battery design, in which the negative electrode, electrolyte, and positive electrode self-segregate into three layers due to immiscibility and the density difference. The natural self-segregation of the three liquid components is beneficial for manufacturing scalability without the employment of brittle solid electrolytes. Moreover, solubility of the Na–K alloy in typical organic electrolytes is negligible at room temperature, which circumvents the self-discharge in molten salt-based high-temperature liquid metal batteries.[18]

Good wetting of liquid metals on current collectors is the prerequisite to build liquid metal batteries.[22] Essentially, wettability is dictated by the balance between adhesive and cohesive forces, in which the former causes the liquid drop to spread out over the solid surface and the latter leads to poor contact.[10] The interaction between liquids and solid substrates and the degree of wetting can be quantified by the Dupré equation and Young–Dupré equation, separately. The wetting behavior of Ga–In on the stainless-steel-based current collector is presented in Figure 1b, and because of the large surface energy (γ_{LG}) of liquid metals, the drop tends to ball up and avoid contact with the surface.[23] According to Young–Dupré equation, enhanced adhesive forces (W_a) between the liquid and the solid is favorable for good wetting. To reinforce the interactions between liquid metals and current collectors, we modified the stainless steel with surface coating of 50 nm Au and 20 nm Al, separately. Figure 1b–d clearly show that the liquid metal wets Au-coated stainless steel better than pristine and Al-coated stainless steel in the Ar atmosphere, and similar wetting behaviors can also be observed when the liquid metal is in direct contact with the organic electrolyte (Figure 1e–g). According to Wenzel's model, the contact angle of a rough surface is different from the intrinsic contact angle of an ideal flat surface following Wenzel's equation. **Figure 2**a–c compares the surface topography of pristine stainless-steel, Au-coated stainless-steel, and Al-coated stainless-steel current collectors. On the one hand, the relatively low roughness of Au-coated stainless steel could contribute to the improved wetting. On the other hand, the density functional theory (DFT) modeling was explored to reveal the effects of adsorption energy. According to the simulation (Table S2, Supporting Information), the adsorption energies between Ga–In atoms and Fe (the main component of stainless steel), Au, and Al_2O_3 (the main component on Al

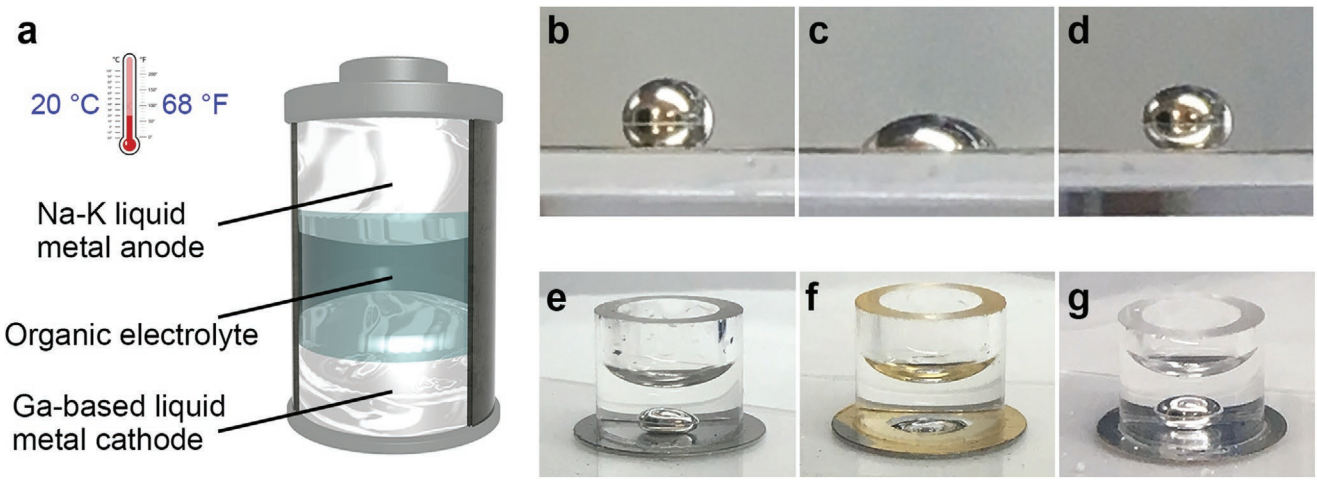

Figure 1. Configuration of the room-temperature liquid metal battery and wetting behavior of Ga–In on current collectors. a) Schematic of the room-temperature liquid metal battery. b) The Ga–In liquid metal on stainless steel. c) The Ga–In liquid metal on Au-coated stainless steel. d) The Ga–In liquid metal on Al-coated stainless steel. e) The Ga–In liquid metal on stainless steel immersed in the Na electrolyte in an Ar-filled glove box. f) The Ga–In liquid metal on Au-coated stainless steel immersed in the Na electrolyte in an Ar-filled glove box. g) The Ga–In liquid metal on Al-coated stainless steel immersed in the Na electrolyte in an Ar-filled glove box.

 © 2020 WILEY-VCH Verlag GmbH & Co. KGaA, Weinheim

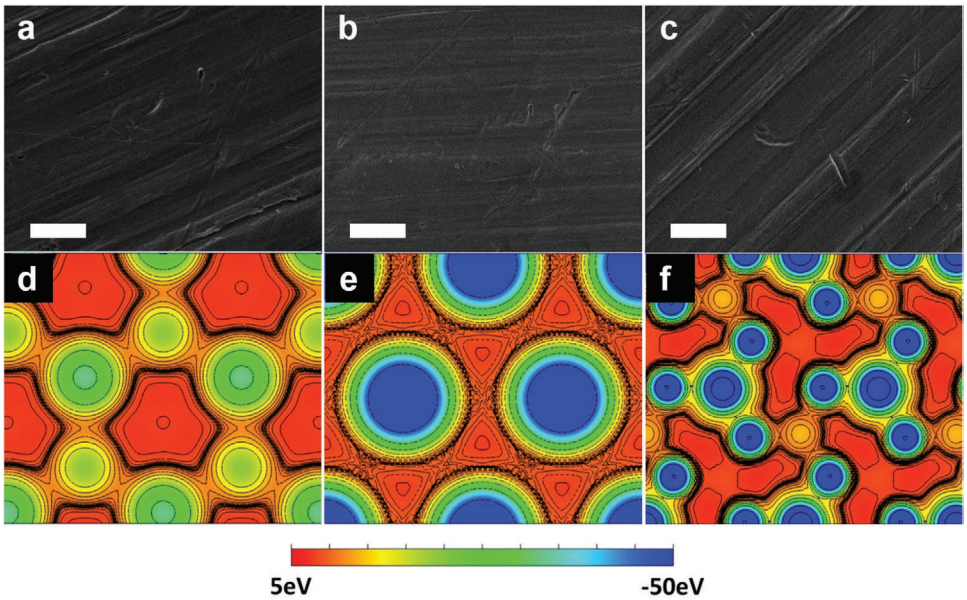

Figure 2. SEM images of current collectors and corresponding DFT modeling of the electrostatic potential maps. a–c) SEM images of: a) the pristine stainless-steel current collector, b) stainless steel coated with Au, and c) stainless steel coated with Al. Scale bar: 20 µm. Calculated electrostatic potential maps of d) the pristine stainless-steel current collector, e) stainless steel coated with Au, and f) stainless steel coated with Al toward Ga–In atoms.

surface) are –0.37, –2.42 , and –0.40 eV, respectively, suggesting that good wetting on Au should be induced by the strong interactions as well. Furthermore, we simulated the electrostatic potential maps of different surfaces toward Ga–In atoms to illustrate the charge distributions and visualize the adsorption capability. As shown in Figure 2d–f, the Au surface maintains more binding sites toward liquid metal atoms, leading to stronger interaction strengths and anchoring effects, which is in good agreement with the experimental results. Moreover, the potential interfacial reactions between liquid metals and substrates may contribute to the improved wetting behavior as well.[24] It should be pointed out that although Au is a precious metal, it is a representative model showing how to address the poor wettability issue of fusible alloys with a combined experimental and computational approach, and such a methodology can be extended to other liquid metals using more cost-effective coating materials.

In addition to controlled wetting, a stable interphase between liquid metals and electrolytes is also required especially considering the high reactivity and fluidity of the Na–K alloy.[25] To immobilize the fluidic liquid metal, a facile vacuum infiltration method is adopted to infuse it into carbon paper-based porous substrates, showing clearly the metallic luster of the matrix (Figure S1a, Supporting Information).[26,27] Nevertheless, the liquid metal is expelled from carbon paper after being immersed into a typical ether-based solvent of dimethoxyethane (DME) (Figure S1b, Supporting Information), which limits direct employment of ether-based electrolytes in liquid metal batteries.[11] Despite the incompatibility between Na–K and DME, a stabilized interphase can be generated when fluoroethylene carbonate (FEC) was added to make a solvent mixture (Figure S1c, Supporting Information). In comparison to DME with a high LUMO energy level of –0.18 eV, FEC maintains a much lower LUMO energy of –0.64 eV, indicating a high tendency to be reduced preferentially (Figure S2, Supporting Information). Accordingly, the formation of F-containing SEI originated from FEC gives rise to the stabilized interphase between the Na–K alloy and the electrolyte.

To gain more insights into the battery chemistry, time-of-flight secondary-ion mass spectrometry (TOF-SIMS) was adopted to analyze Na–K and the Na electrolyte interface layer. TOF-SIMS is well suited for surface and buried interface characterization given its powerful analytical capabilities with sub-nanoscale sensitivity, ultralow detection limits, high mass resolution, and depth profiling functions with atomic depth resolution.[28,29] Here, the interface layer on liquid metals is directly visualized, as shown in **Figure 3**, where various species (i.e., secondary ions) of interest are identified, located, and relatively quantified. The normalized (to their maximum) depth profiles in Figure 3a reveal the dual-layer characteristics of the interphase containing various components. The outer layer of the surface is comprised of both organic and inorganic species, while the inner layer close to alkali metals mainly contains inorganic products. Such a special dual-layer structure correlates with the generally accepted mosaic model of SEI, in which the salt and solvent decomposition products will first deposit on the electrode surface after initial nucleation in the outer region and then be further reduced into inorganic products in the inner region.[5,30,31] Therefore, such an interphase contributes to the immobilization of Na–K liquid alloy in the porous structure of carbon paper. In contrast, the pristine Na–K alloy has a much simpler surface chemistry without the dual-layer characteristics (Figure S3, Supporting Information). Due to the highly reactive nature of alkali metals, the surface film of pristine Na–K should be slightly evolved from the reaction between Na–K and trace amount of impurities in the Ar-filled glove box.

 © 2020 WILEY-VCH Verlag GmbH & Co. KGaA, Weinheim

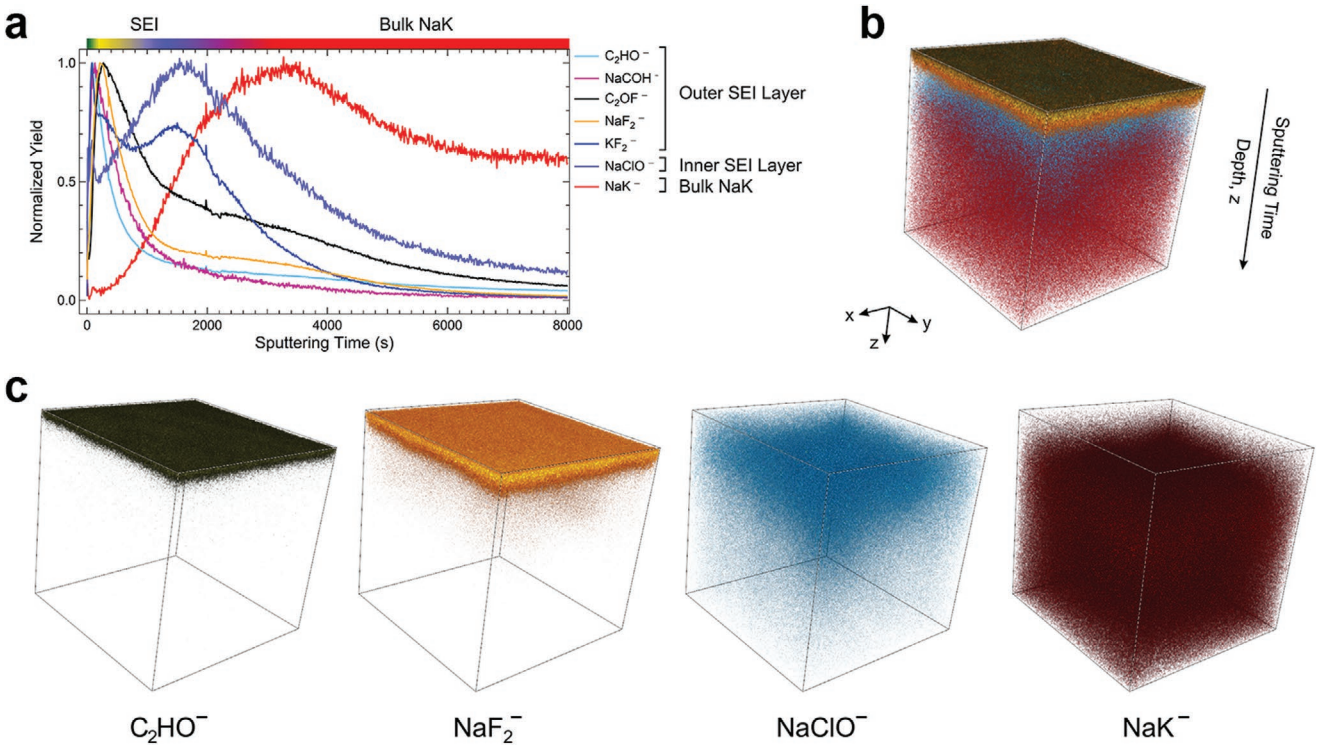

Figure 3. TOF-SIMS analysis of the Na–K/Na electrolyte interface layer. a) Normalized (to their maximum) depth profiles of various secondary ions of interest contained in the sputtered volume at the Na–K/electrolyte interface. b) 3D, multicolor overlay of representative secondary ions composing the different layers of the interface. c) Individual spatial distributions of the selected secondary ions (C_2HO^-, NaF_2^-, $NaClO^-$, and NaK^-) overlaid in (b).

Consequently, the intensities of the selected secondary ions at the Na–K surface are much lower than at the Na–K/electrolyte interface (Figure S4, Supporting Information). Figure 3b,c demonstrate three dimensionally the stratified localization of the representative secondary ion fragments contained in the sputtered volume at the Na–K/electrolyte interface, whereby reversible redox reactions of liquid metals can be expected in the presence of such an interphase.

With the improved wetting behavior and the stabilized interface layer, a room-temperature liquid metal battery was built using an Na–K negative electrode and a Ga–In positive electrode. **Figure 4**a presents the cyclic voltammogram of the Ga–In‖Na–K liquid metal battery, and the two pairs of redox peaks should be ascribed to the sodiation of Ga and In successively, which correlates with the plateaus in Figure 4b as well. For comparison, the cyclic voltammogram of the Ga‖Na–K cell is shown in Figure S5, Supporting Information, and only one pair of redox peaks is observed during the same potential range, indicating the sole redox characteristics of Ga. The cyclic voltammograms of In‖Na–K and Sn‖Na–K cells are presented in Figures S6 and S7, Supporting Information. It is noted that the discharge voltage of In is located at ≈0.33 V, while the discharge voltage of Sn is located at 0.44, 0.39, and 0.26 V. Therefore, in the cutoff potential of 0.4–1 V, In contributes little to the capacity of the Ga–In‖Na–K cell, while Sn should make a contribution to the total capacity of the Ga–Sn‖Na–K cell. Because of the intrinsically high density of Ga–In, the volumetric capacity can reach 491 mAh cm^{-3} at 1 C (1 C = 100 mA g^{-1}) based on the volume of the electrode. Figure S8, Supporting Information shows the cycling performance of Ga–In‖Na–K with a wide potential window between 0.1 and 1 V, and the capacity decay could be attributed to the discounted self-healing capabilities under such a low discharge cutoff potential with relatively large volume change and solid phase formation. Herein, we narrowed the potential window to 0.4–1 V, and only the first sodiation/desodiation reaction was utilized in Figure 4a, which corresponds to the alloying and dealloying reaction between Ga and Na. In the meantime, the deposition of Ga on the negative electrode can also be avoided within the cutoff potential range. Owing to the fast charge transfer kinetics at the liquid electrode–liquid electrolyte interface, decent rate capabilities were demonstrated as presented in Figure 4c. In addition to fast kinetics, the self-healing nature of liquid metals renders the cell immune to dendrites or cracks faced with conventional solid-state electrodes. Capacity retention of 99.95% per cycle is achieved with stabilized Coulombic efficiency of ≈100% (Figure 4d). In contrast, when replacing the Na electrolyte with a K electrolyte, Ga–In shows almost no capacities (Figure S9, Supporting Information), indicating electrochemical inactivity of Ga–In toward K ions. Considering the coexistence of Na and K in the negative electrode, the reversible and stable stripping/deposition of Na in the negative electrode relies on the Na-containing interphase as verified by the TOF-SIMS analysis.[26] We also tested the Ga–In electrode versus an Na anode with a cutoff voltage between 0.01 and 1 V, as shown in Figure S10, Supporting Information. The capacity decays very quickly with the retention of 19.3% after 100 cycles, which should be ascribed to the dendritic growth of the Na anode and instable interfaces of both the anode and cathode with continuous electrolyte decomposition.

 © 2020 WILEY-VCH Verlag GmbH & Co. KGaA, Weinheim

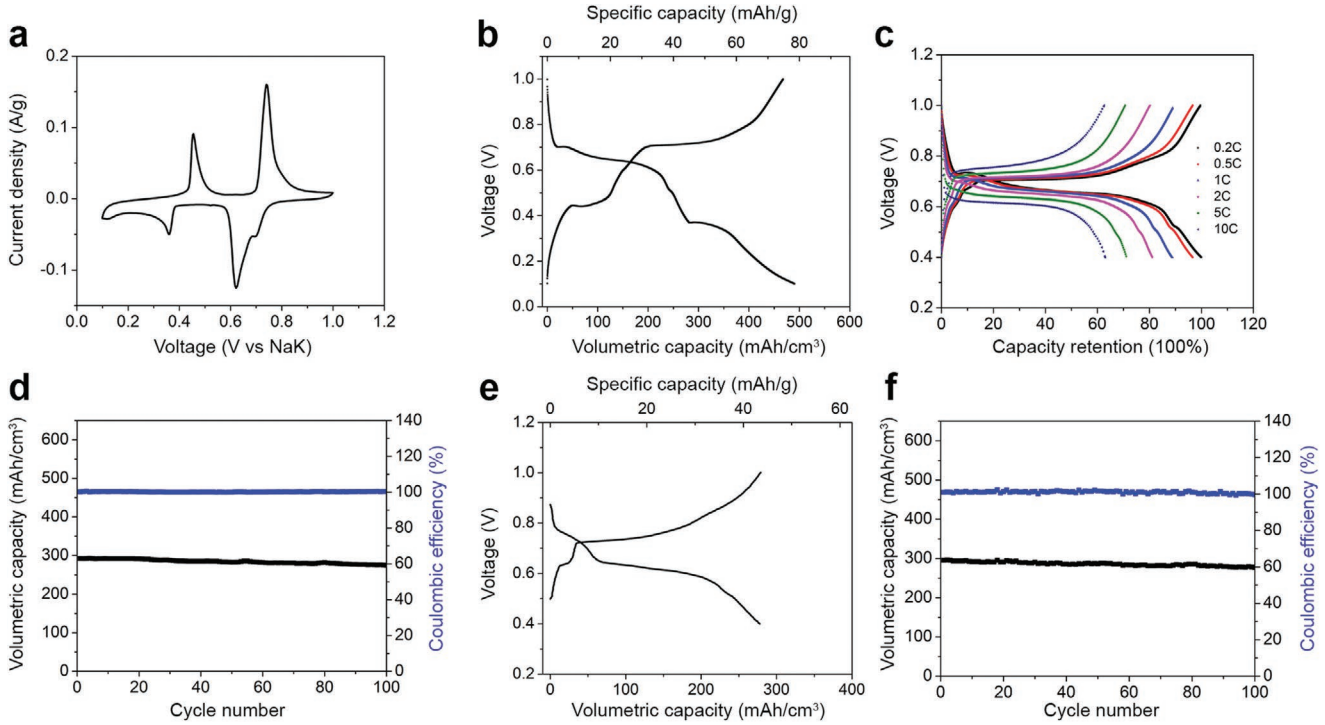

Figure 4. Cell performance of room-temperature liquid metal batteries. a) Cyclic voltammogram of the Ga–In||Na–K liquid metal battery at a scan rate of 0.05 mV s^{-1} in the Na electrolyte. b) Galvanostatic charge–discharge voltage profiles of the Ga–In||Na–K liquid metal battery at 1C in the Na electrolyte. c) Rate capability of the Ga–In||Na–K liquid metal battery in the Na electrolyte. d) Cycling stability of the Ga–In||Na–K liquid metal battery at 1C in the Na electrolyte. e) Galvanostatic charge–discharge voltage profiles of the Ga–Sn||Na–K liquid metal battery at 1C in the Na electrolyte. f) Cycling stability of the Ga–Sn||Na–K liquid metal battery at 1C in the Na electrolyte.

Moreover, the operating temperature of liquid metal batteries can be further lowered by extending the battery chemistry to other fusible alloys. Figures S11 and S12, Supporting Information show the charge–discharge voltage profiles and cycling performance of Galinstan versus Na–K, with the former maintaining a melting point of –19 °C. Despite the ternary eutectic alloy containing Ga, In, and Sn in Galinstan, the similar potential plateau with that of Ga–In proves that the electrochemical reaction mainly relies on Ga. In view of the low abundance of In, we can also decrease the cost of liquid metal systems by replacing In with Sn, and the performance of the Ga–Sn||Na–K liquid metal battery is presented in Figure 4e,f. In addition to voltage profiles, Ga–Sn||Na–K cell also maintains similar cycling stability and Coulombic efficiency. The charge–discharge voltage profiles of the liquid metal batteries for the first cycle were provided in Figures S13 and S14, Supporting Information. The comparable electrochemical properties and cycling stability of Ga–In, Ga–Sn, and Galinstan demonstrate the universal characteristics of Ga-based fusible alloys for energy storage applications. Table S3, Supporting Information further summarizes the energy density of all three prototypes of room-temperature liquid metal batteries ranging from 134 to 181 Wh L^{-1}, which is comparable to or even higher than reported high-temperature liquid metal systems and nearly one order of magnitude larger than other typical grid-scale energy storage devices, such as redox flow batteries.[15,20] A transparent cell of the liquid metal battery was further built (Figure S15, Supporting Information). No dendrites can be observed in the Na–K liquid metal, and no cracks can be detected in the Ga–Sn liquid metal. Moreover, the SEM image of the Ga–Sn liquid metal after sodiation was taken, and it is noted that the Ga–Sn and electrolyte interface is very stable even after cycling (Figure S16, Supporting Information). To demonstrate the effect of good wetting on the cell performance, a transparent cell was assembled using stainless steel as the current collector (Figure S17, Supporting Information), and it is noted that the Ga–Sn liquid metal balls up on the current collector. Meanwhile, the liquid metal cannot be immobilized, and it tends to roll around (Figure S17, right, Supporting Information), which may further affect the charge transport between the liquid metal and the current collector. The electrochemical test also shows that such a cell can hardly work at a current density of 100 μA cm^{-2} (Figures S18 and S19, Supporting Information).

To gain more insights into the phase behavior of liquid metals during cell operation, the XRD patterns were collected before and after sodiation (Figure S20, Supporting Information). The minor peaks at ≈34° correspond to the existence of pristine liquid metals, and it is noted that the signature patterns of all liquid metals disappeared after sodiation, suggesting the possible phase transformation from liquids to solids.[32,33] The emerged peaks at ≈45° in the sodiated Ga–In sample also indicate the solid-state discharge products. Nevertheless, no noticeable new peaks can be observed in Ga–Sn or galinstan. And it might be due to the amorphous feature of discharged products in the presence of Sn and will be investigated further more in the future. The sodiated product of Ga-based liquid metals

© 2020 WILEY-VCH Verlag GmbH & Co. KGaA, Weinheim

maintains a high melting point as a result of the ionic bond character considering the large difference in the electronegativities of Ga and Na. Therefore, the all-liquid-metal battery is only maintained in a fully charged state. In the meantime, the solid phase can be self-healed when the cell is charged with liquid phase regenerated, which correlates to the self-healing nature of liquid metals.

In addition to the performance characteristics mentioned above, safety is always of the utmost importance when implementing batteries for practical applications.[34] Although the potential safety issues related to dendrite growth of alkali metals can be eliminated using liquid electrodes, the violent reactions between fluidic negative electrodes and positive electrodes may give rise to another safety concern, especially in high-temperature liquid metal batteries, such as Na-S cells.[10] Here, a puncture test was conducted to evaluate the safety performance of our room-temperature liquid metal cells. Figure S21a,b, Supporting Information shows the photograph and the IR image of the Ga–In liquid metal in an Ar-filled glove box, and the temperature was detected to be ≈30 °C. It is notable that the temperature remained almost unchanged when Ga–In got in touch with the Na–K liquid alloy (Figure S22a,b, Supporting Information), which should be due to the insulating layer formed on the liquid metal surface. Both the unchanged temperature and segregated phases when mixing the liquid metal negative electrode and positive electrode suggest the high safety margin of such room-temperature liquid metal batteries. Besides, we narrowed the potential window to 0.4–1 V, and only the alloying and dealloying reactions between Ga and Na take place. Therefore, the deposition of Ga on the negative electrode can be prevented within such a cutoff potential range.

Figure 5 compares the operating temperature of typical liquid metal batteries reported so far.[15,18] It is obvious that most of the cells can only operate above 400 °C to maintain the molten state of metals. The lowest operating temperature in published reports up to now is 240 °C by Cui et al. employing Bi–Pb or Sn–Pb versus Li.[18] Although this intermediate temperature is compatible with polymer sealing, it is still not friendly in other applications except for grid energy storage, and the brittle solid electrolyte further complicates the cell assembly process and increases the capital cost. In contrast, we demonstrate the first-of-its-kind room-temperature liquid metal battery by employing fusible alloys as both the positive and negative electrode, whereby the operating temperature is expected to be decreased below melting point of water when a ternary alloy of Ga–In–Sn (Galinstan) is adopted, suggesting the potential applications in harsh environments. In the meantime, the extra cost on thermal management, special maintenance, seals, and corrosion in high-temperature liquid metal batteries can all be reduced remarkably.

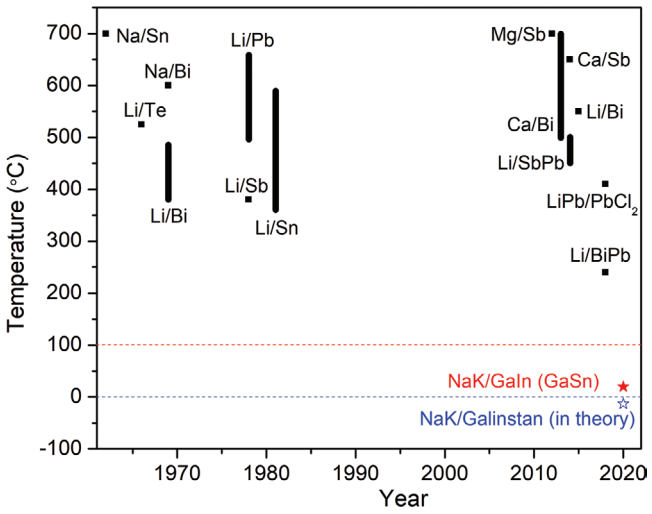

Figure 5. Comparison of operating temperature of different liquid metal batteries.

The liquid metal battery system is also analyzed in terms of cost. Figures S23 and S24, Supporting Information give the abundance of chemical elements in the solar system and Earth's crust, separately, and it is noted that Na and K, both of which are the main components in the negative electrode, are much more abundant than Li.[35] Actually, the Earth's crust contains 2.3 wt% of Na and 1.5 wt% of K, making them the seventh and eighth most abundant elements, respectively. Moreover, both Na and K can also be extracted from the ocean, and the abundance is estimated to be 1.1 wt% for Na and 0.042 wt% for K.[36] Whereas, the crustal and oceanic abundance of Li is merely 0.0017 and 0.000018 wt%.[37] Although Ga, the main component in the fusible positive electrode alloy, is not as abundant as Na, the abundance is still comparable with Ni and Cu and larger than Co, Sn, and Pb in Earth's crust. We also built the Ga–Sn||Na–K cell to eliminate the use of the rare metal of In, and Sn is a major industrial metal widely used already. And it should be pointed out that due to the special geochemical behavior of Ga, it rarely forms high-content ore deposits as a primary source. Because Ga is mainly produced from minerals as a by-product during the extraction of other metals, now its market price relies on the market conditions of the main products, and its relatively high crustal abundance indicates the potential great supply and low cost in the future. Besides, Ga-based alloys are adopted here to show the great promise of fusible alloy family for energy storage systems, and some other cost-effective alternatives can also be explored to build the liquid metal batteries, as shown in Table S1, Supporting Information. Hg is a common liquid metal at room temperature, which has been used in thermometers. Nevertheless, the widespread application of Hg in energy systems is limited by its high toxicity. Therefore, the Bi-based fusible alloys, typically maintaining a melting point between 40 and 100 °C, represent another promising type of electroactive materials to build low-temperature liquid metal batteries.

On the other hand, the battery system should be evaluated in terms of environmental consequence and human risk as well. Actually the widespread implementation of lead acid batteries is partly restricted by the serious environmental concerns considering the high toxicity of lead compounds. In this respect, the nontoxic Ga-based alloys are more environmentally friendly in comparison with the Pb-containing alloys in high-temperature liquid metal batteries reported recently.[17,18] Accordingly, the hazards of heavy metal contamination and the potential threats to human health can be circumvented. Most organic electrolytes may cause some safety concerns, especially fluorine-containing ones. The amount of fluorine in our electrolyte is much lower

© 2020 WILEY-VCH Verlag GmbH & Co. KGaA, Weinheim

than hexafluorophosphate-based electrolytes, and the price is also lower than typical solid electrolytes. The Na–K liquid metal is compatible with the K-alumina-based solid electrolyte as well, which may be a promising electrolyte alternative provided the production cost can be lowered further.

With rational selection of the fusible alloys and comprehensive study on the wetting behavior and interfacial chemistry, the first-of-its-kind room-temperature liquid metal battery was developed, with great potential to further decrease the operating temperature below 0 °C when using the Ga–In–Sn ternary alloy-based positive electrode. Thanks to the enhanced solid–liquid adhesion energy on the Au-coated current collector, good wetting of liquid metals is achieved. Further interfacial chemistry study reveals that a stable interphase is generated between the liquid Na–K alloy and electrolytes, and the dual-layer structure visualized by TOF-SIMS plays a critical role in regulating the reversible stripping/deposition of Na ions. In addition to the reduced cost on thermal management and cell maintenance, the room-temperature liquid metal battery also circumvents the concerns arising from brittle and costly solid electrolytes or the self-discharge issue using molten salt-based electrolytes in conventional high-temperature liquid metal batteries. In the proof-of-concept cell test, the Ga–In-based liquid metal battery maintains capacity retention of 99.95% per cycle with stabilized Coulombic efficiency of ≈100%, and similar electrochemical performance was demonstrated in cases of Ga–Sn and Galinstan-based liquid metal batteries at room temperature. In addition to grid-scale energy storage like typical high-temperature liquid metal batteries, such room-temperature liquid metal batteries can also be applied for bendable and wearable electronic devices considering the high flexibility and even stretchability of liquid metals. Despite the relatively high market price of Ga-based alloys at the present stage, they represent a promising family of fusible alloys for energy storage devices, and other cost-effective alternatives, as shown in Table S1, Supporting Information, can also be potentially useful for high-performance room-temperature liquid batteries. This work not only shows how to broaden the liquid metal battery chemistries with wide selection of liquid metal electrodes and electrolytes, but also extends the potential applications beyond stationary storage.

Supporting Information

Supporting Information is available from the Wiley Online Library or from the author.

Acknowledgements

Y.D. and X.G. contributed equally to this work. G.Y. acknowledges the financial support from Camille Dreyfus Teacher–Scholar Award, Sloan Research Fellowship, and the Welch Foundation Award F-1861.

Conflict of Interest

The authors declare no conflict of interest.

Keywords

interfacial chemistry, liquid metals, Na-ion batteries, room temperature, smart grid

Received: April 15, 2020
Revised: May 18, 2020
Published online:

[1] J. B. Goodenough, *Energy Environ. Sci.* **2014**, *7*, 14.
[2] K. Kirshenbaum, D. C. Bock, C.-Y. Lee, Z. Zhong, K. J. Takeuchi, A. C. Marschilok, E. S. Takeuchi, *Science* **2015**, *347*, 149.
[3] D. Lin, Y. Liu, Y. Cui, *Nat. Nanotechnol.* **2017**, *12*, 194.
[4] X. Guo, Y. Ding, H. Gao, J. Goodenough, G. Yu, *Adv. Mater.* **2020**, *32*, 2000316.
[5] X.-B. Cheng, R. Zhang, C.-Z. Zhao, Q. Zhang, *Chem. Rev.* **2017**, *117*, 10403.
[6] J. Bae, Y. Qian, Y. Li, X. Zhou, J. Goodenough, G. Yu, *Energy Environ. Sci.* **2019**, *12*, 3319.
[7] C.-P. Yang, Y.-X. Yin, S.-F. Zhang, N.-W. Li, Y.-G. Guo, *Nat. Commun.* **2015**, *6*, 8058.
[8] Z. Zeng, V. Murugesan, K. S. Han, X. Jiang, Y. Cao, L. Xiao, X. Ai, H. Yang, J.-G. Zhang, M. L. Sushko, J. Liu, *Nat. Energy* **2018**, *3*, 674.
[9] G. Zheng, S. W. Lee, Z. Liang, H.-W. Lee, K. Yan, H. Yao, H. Wang, W. Li, S. Chu, Y. Cui, *Nat. Nanotechnol.* **2014**, *9*, 618.
[10] X. Lu, G. Li, J. Y. Kim, D. Mei, J. P. Lemmon, V. L. Sprenkle, J. Liu, *Nat. Commun.* **2014**, *5*, 4578.
[11] L. Xue, W. Zhou, S. Xin, H. Gao, Y. Li, A. Zhou, J. B. Goodenough, *Angew. Chem., Int. Ed.* **2018**, *57*, 14184.
[12] Y. Wu, L. Huang, X. Huang, X. Guo, D. Liu, D. Zheng, X. Zhang, R. Ren, D. Qu, J. Chen, *Energy Environ. Sci.* **2017**, *10*, 1854.
[13] M. B. Ghasemian, M. Mayyas, S. A. Idrus-Saidi, M. A. Jamal, J. Yang, S. S. Mofarah, E. Adabifiroozjaei, J. Tang, N. Syed, A. P. O'Mullane, T. Daeneke, K. Kalantar-Zadeh, *Adv. Funct. Mater.* **2019**, *29*, 1901649.
[14] K. Kalantar-Zadeh, J. Tang, T. Daeneke, A. P. O'Mullane, L. A. Stewart, J. Liu, C. Majidi, R. S. Ruoff, P. S. Weiss, M. D. Dickey, *ACS Nano* **2019**, *13*, 7388.
[15] H. Kim, D. A. Boysen, J. M. Newhouse, B. L. Spatocco, B. Chung, P. J. Burke, D. J. Bradwell, K. Jiang, A. A. Tomaszowska, K. Wang, W. Wei, L. A. Ortiz, S. A. Barriga, S. M. Poizeau, D. R. Sadoway, *Chem. Rev.* **2013**, *113*, 2075.
[16] X. Guo, L. Zhang, Y. Ding, J. B. Goodenough, G. Yu, *Energy Environ. Sci.* **2019**, *12*, 2605.
[17] K. Wang, K. Jiang, B. Chung, T. Ouchi, P. J. Burke, D. A. Boysen, D. J. Bradwell, H. Kim, U. Muecke, D. R. Sadoway, *Nature* **2014**, *514*, 348.
[18] Y. Jin, K. Liu, J. Lang, D. Zhuo, Z. Huang, C.-a. Wang, H. Wu, Y. Cui, *Nat. Energy* **2018**, *3*, 732.
[19] X. Guo, Y. Ding, L. Xue, L. Zhang, C. Zhang, J. B. Goodenough, G. Yu, *Adv. Funct. Mater.* **2018**, *28*, 1804649.
[20] Y. Ding, C. Zhang, L. Zhang, Y. Zhou, G. Yu, *Chem. Soc. Rev.* **2018**, *47*, 69.
[21] R. W. Ohse, *Handbook of Thermodynamic and Transport Properties of Alkali Metals*, Blackwell Scientific Publications, Oxford, UK **1985**.
[22] Y. Ding, X. Guo, Y. Qian, H. Gao, D. Weber, L. Zhang, J. Goodenough, G. Yu, *Angew. Chem., Int. Ed.* **2020**, https://doi.org/10.1002/anie.202005009.
[23] Y.-G. Park, H. Min, H. Kim, A. Zhexembekova, C. Y. Lee, J.-U. Park, *Nano Lett.* **2019**,*19*, 4866.
[24] J. Wang, H. Wang, J. Xie, A. Yang, A. Pei, C.-L. Wu, F. Shi, Y. Liu, D. Lin, Y. Gong, Y. Cui, *Energy Storage Mater.* **2018**, *14*, 345.
[25] L. Xue, H. Gao, W. Zhou, S. Xin, K. Park, Y. Li, J. B. Goodenough, *Adv. Mater.* **2016**, *28*, 9608.

 © 2020 WILEY-VCH Verlag GmbH & Co. KGaA, Weinheim

[26] Y. Ding, X. Guo, Y. Qian, L. Zhang, L. Xue, J. B. Goodenough, G. Yu, *Adv. Mater.* **2019**, *31*, 1806956.
[27] J. Wan, J. Song, Z. Yang, D. Kirsch, C. Jia, R. Xu, J. Dai, M. Zhu, L. Xu, C. Chen, Y. Wang, Y. Wang, E. Hitz, S. D. Lacey, Y. Li, B. Yang, L. Hu, *Adv. Mater.* **2017**, *29*, 1703331.
[28] X. Fan, X. Ji, F. Han, J. Yue, J. Chen, L. Chen, T. Deng, J. Jiang, C. Wang, *Sci. Adv.* **2018**, *4*, eaau9245.
[29] H. Chou, A. Ismach, R. Ghosh, R. S. Ruoff, A. Dolocan, *Nat. Commun.* **2015**, *6*, 7482.
[30] Y. Sun, N. Liu, Y. Cui, *Nat. Energy* **2016**, *1*, 16071.
[31] R. Zhang, N.-W. Li, X.-B. Cheng, Y.-X. Yin, Q. Zhang, Y.-G. Guo, *Adv. Sci.* **2017**, *4*, 1600445.
[32] A. D. Pelton, S. Larose, *Bull. Alloy Phase Diagrams* **1990**, *11*, 347.
[33] M. V. Dergacheva, E. G. Shatrova, O. V. Kharina, *Russ. J. Phys. Chem.* **1996**, *70*, 204.
[34] Z. Chen, P.-C. Hsu, J. Lopez, Y. Li, J. W. F. To, N. Liu, C. Wang, Sean C. Andrews, J. Liu, Y. Cui, Z. Bao, *Nat. Energy* **2016**, *1*, 15009.
[35] H. Wang, C. Wang, E. Matios, W. Li, *Angew. Chem., Int. Ed.* **2018**, *57*, 7734.
[36] W. Luo, F. Shen, C. Bommier, H. Zhu, X. Ji, L. Hu, *Acc. Chem. Res.* **2016**, *49*, 231.
[37] J. Lang, Y. Jin, K. Liu, Y. Long, H. Zhang, L. Qi, H. Wu, Y. Cui, *Nat. Sustain* **2020**, *3*, 386.

© 2020 WILEY-VCH Verlag GmbH & Co. KGaA, Weinheim